# Velodyne HDL-64E lidar for unmanned surface vehicle obstacle detection

Ryan Halterman, Michael Bruch

Ryan Halterman, Michael Bruch, "Velodyne HDL-64E lidar for unmanned surface vehicle obstacle detection," Proc. SPIE 7692, Unmanned Systems Technology XII, 76920D (7 May 2010); doi: 10.1117/12.850611

SPIE.

Event: SPIE Defense, Security, and Sensing, 2010, Orlando, Florida, United States

# Velodyne HDL-64E LIDAR for Unmanned Surface Vehicle Obstacle Detection

Ryan Halterman, Michael Bruch
Space and Naval Warfare Systems Center, Pacific

## ABSTRACT

The Velodyne HDL-64E is a 64 laser 3D (360×26.8 degree) scanning LIDAR. It was designed to fill perception needs of DARPA Urban Challenge vehicles. As such, it was principally intended for ground use. This paper presents the performance of the HDL-64E as it relates to the marine environment for unmanned surface vehicle (USV) obstacle detection and avoidance. We describe the sensor's capacity for discerning relevant objects at sea—both through subjective observations of the raw data and through a rudimentary automated obstacle detection algorithm. We also discuss some of the complications that have arisen with the sensor.

**Keywords:** Velodyne, HDL-64E, LIDAR, unmanned surface vehicle, USV, obstacle detection, marine

## 1. INTRODUCTION

One of the primary perception tasks for a mobile unmanned system entails detection of potential obstacles within an area of interest. Sensors commonly employed for this task include passive-ranging cameras (in monocular and stereo configurations), and active-ranging SONAR, RADAR, and LIDAR. Cameras using real-time techniques typically provide high lateral and temporal resolution, but relatively low depth resolution and accuracy. Active-ranging sensors are able to provide high depth resolution and accuracy, but commonly do so with only a single beam—the size of which may vary greatly by specific type. To image a scene, sensors often scan this beam along one or two axes. In addition to differences in beam width, which determines the sensor's resolving capability, these sensors vary greatly in their one and two axis scan rates, pulse rates, and effective ranges.

Interplay between these properties determines the sensor's resolution, its three-dimensional field of view, and the density of coverage within that field of view. Because of their particular combination of these characteristics, two and three-dimensional scanning LIDARs are frequently used for short-to-medium range obstacle avoidance on unmanned vehicles that can accommodate the size, power, weight, and complexity of an active sensor.

The Velodyne HDL-64E[1] is a 3D scanning LIDAR. Using 64 separate lasers, it provides a 360° horizontal field of view (FOV) at 0.09° incremental postings. Vertically, the 64 lasers are arranged to cover the range from −24.8° to +2° at approximately 0.4° increments. It was developed subsequent to the Defense Advanced Research Projects Agency (DARPA) Grand Challenge competitions of 2004 and 2005. In the 2007 DARPA Urban Challenge, 12 teams made use of the sensor including the top two finishers, Tartan Racing[2]and Stanford Racing.[3]

The usefulness of three-dimensional LIDAR-scanned data for object and terrain detection, tracking, and modeling is contingent on a number of factors. Among these are the following: scanning rate and density; coverage in azimuth, elevation, and range; inherent sensor noise; calibration error; and sensitivity to environmental conditions. This paper presents observations of HDL-64E use in a marine environment with regard to these factors. First we present data illustrating general detail in marine-relevant objects at various ranges. Next, we briefly discuss a simple autonomous obstacle detection algorithm for unmanned sea surface vehicles. Finally, we discuss some of the complications that have arisen over the course of operation of the sensor.

Unmanned Systems Technology XII, edited by Grant R. Gerhart, Douglas W. Gage, Charles M. Shoemaker,
Proc. of SPIE Vol. 7692, 76920D · © 2010 SPIE · CCC code: 0277-786X/10/$18 · doi: 10.1117/12.850611

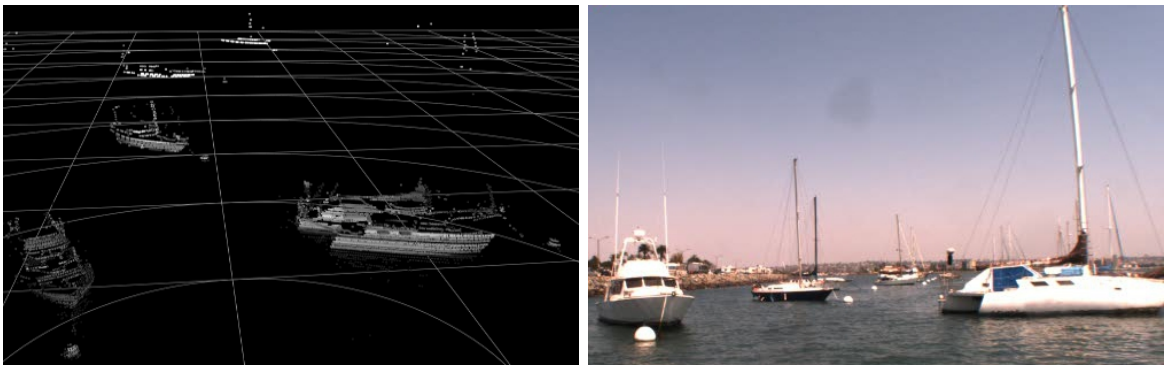

(a) Laser return intensity (b) Photo

Figure 1: Intensity imaging quality of moored boats including trimaran sailboat, power boat, and mono-hull sailboats.

## 2. OBJECT DETAIL AT VARIOUS RANGES

The following section illustrates the discernment quality of data collected from the HDL-64E for maritime objects of interest at various ranges including recreational boats, kayaks, navigation buoys, small lobster trap buoys, partially submerged rocks, floating kelp, and returns from the water surface itself. The test platform is composed of an HDL-64E mounted about 3 meters above the sea surface aboard a 20 foot Seadoo Challenger 2000 sport boat. For the collections shown here, the LIDAR was mounted on a camera stabilization platform to limit roll and pitch motion and the platform speed was generally limited to less than 10 knots. All raw LIDAR returns are plotted on a 10 meter grid.

### 2.1 Boats

Figure 1 illustrates the discernment capability of the HDL-64E. It shows intensity returns for a group of moored boats of different types. Vessel type is easily distinguished at near range including hull-type. The trimaran sailboat in the lower right, the power boat in the lower left and the other mono-hull sailboats are all visible. Even for the farthest boat (approximately 90 meters) imaged, several returns from the mast distinguish it as a sailboat. The limited vertical field of view prohibits any returns from the mast of the nearby trimaran, however.

### 2.2 Kayaks

Besides commercial ships and recreational power and sailboats, USVs operating in the littoral zone may encounter kayaks, canoes, rafts, and other similar small craft. Figures 2a-2e show a pair of kayaks imaged by the HDL-64E at various ranges and 2f presents a photo of the imaged kayaks. The maximum range at which LIDAR returns are persistently present for these kayaks occurs at approximately 90 meters. At this range, there are only about three returns per kayak and no discriminatory information. By 70 meters (Figure 2b) the basic hull shape is present and at 40 meters there are several returns from the paddles and paddlers. At 10 meters, the shaft of the paddle is clearly discernible in the trailing kayak.

### 2.3 Buoys

Navigation buoys, an important fixed obstacle in maritime environments, often have somewhat unique physical properties. As seen in Figure 3f, the buoy considered here has a set of corner-reflectors raised on posts above a cylindrical base. This particular one is relatively smooth and brightly colored. Figure 3a shows the navigation buoy as seen at approximately 100 meters. There are good returns from all parts of the buoy and its general shape is represented, if roughly so. By 70 meters (Figure 3b), much more of the buoy's shape is apparent. We also begin to see what appear to be misplaced returns (purple) due to the corner reflecting top of the buoy. The corner-reflector-scattered returns become more apparent as the buoy gets closer (Figures 3c-3e) and scattered points from both the upper *and* lower corner-reflectors appear.

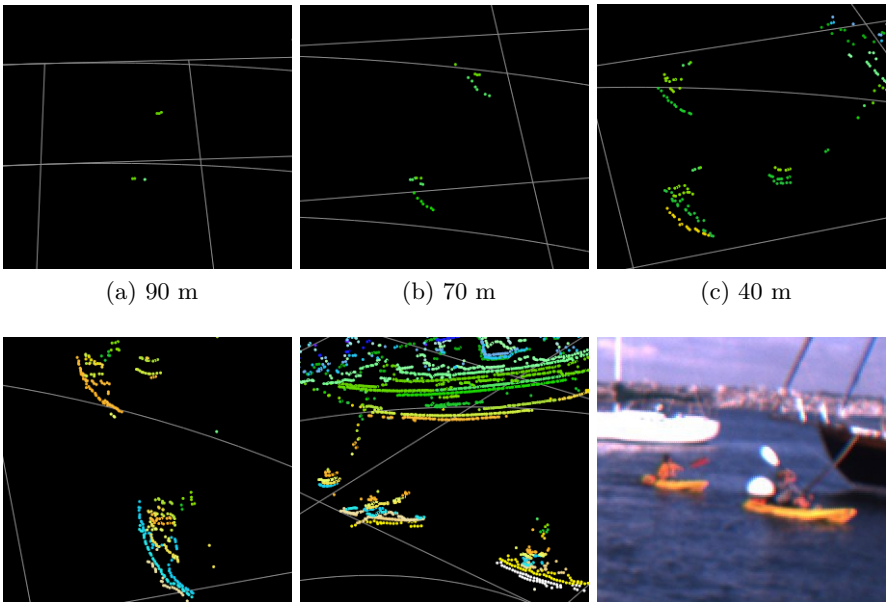

(a) 90 m (b) 70 m (c) 40 m

(d) 20 m (e) 10 m (f) Photo

Figure 2: Two kayaks observed at different ranges

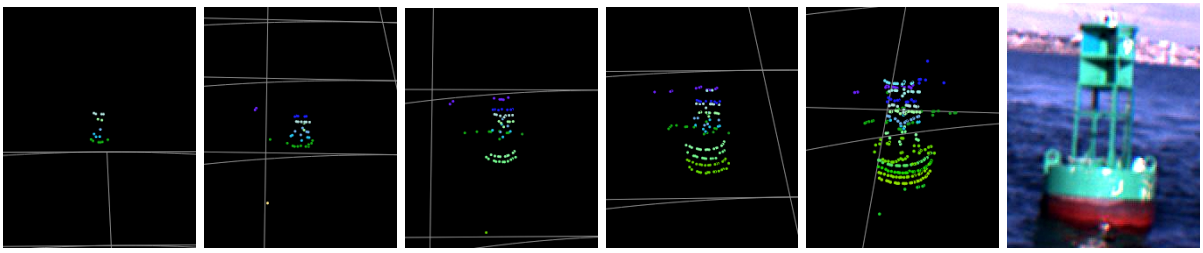

(a) 100 m (b) 70 m (c) 55 m (d) 40 m (e) 25 m (f) Photo

Figure 3: Navigation buoy at different ranges

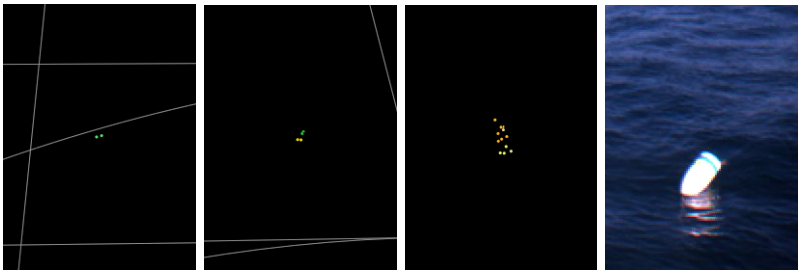

(a) 40 m (b) 25 m (c) 15 m (d) Photo

Figure 4: Return from lobster trap float at different ranges

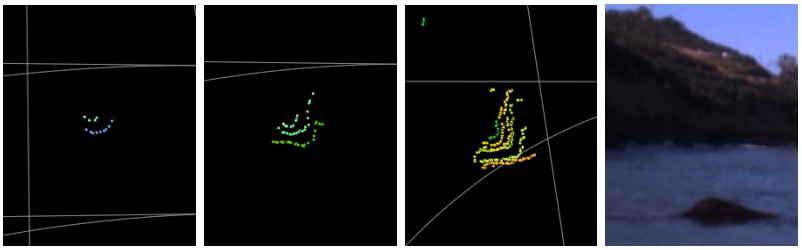

(a) 65 m (b) 35 m (c) 20 m (d) Photo

Figure 5: Return from partially-submerged black rock at varied ranges

At the other end of the size spectrum for buoys are lobster trap buoys (Figure 4d). They represent the class of small floating obstacles of varying navigational severity. This buoy is detected first at approximately 40 meters with only two laser returns (Figure 4a). It is not until 15 meters that any appreciable object shape is apparent.

### 2.4 Partially-submerged rock

Other potentially severe risks to surface vehicles are submerged and partially submerged obstacles. This is especially true for operation in the littoral zone where such occurrences are more likely. The infrared lasers of the HDL-64E are largely unable to penetrate the ocean surface at the incidence angles present in the most common horizontal-sweeping sensor orientation. The only evidence of submerged obstacles detectable by the sensor lies in their partially extending above the surface. Figure 5d shows a dark colored, partially submerged rock near the coast. It is imaged by the Velodyne LIDAR in Figures 5a, 5b, and 5c at 65, 35, and 20 meters respectively.

### 2.5 Water surface returns

In general, the HDL-64E reports no return from the sea surface. Figures 6 and 7 illustrate two common exceptions. Figure 6b shows a photo of the water surface aerated by the recent passage of a small, slow moving, propeller-driven boat. This same wake is imaged by the LIDAR in Figure 6a; the stern of the boat is visible at the far right edge of the figure. It also shows the wake behind the faster moving test platform in the lower left quarter of the image. The speed dependency of the wake contour is apparent in the LIDAR imagery.

Kelp at or near the ocean surface appears, in HDL-64E data, rather similar to aerated water, though somewhat more sparse. Figure 7a shows the return from an area of surface-lying kelp and Figure 7b a photo of the same area. The dense patch seen in the lower right corner of the photo corresponds to the cluster of returns at a range of about 12 meters and a bearing of about 30° from the USV test platform.

## 3. AUTOMATED OBSTACLE DETECTION

Because, as evidenced above, most maritime obstacles appear clearly and most of the sea surface provides no return in HDL-64E data, the primary challenge for obstacle detection lies in limiting false positives caused by

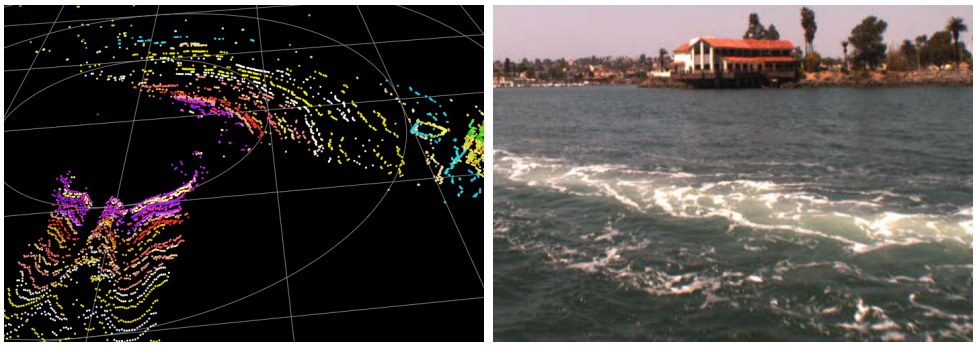

(a) Return from wake (b) Photo of wake

Figure 6: Laser return from water aerated by the recent passage of a small propeller-driven boat.

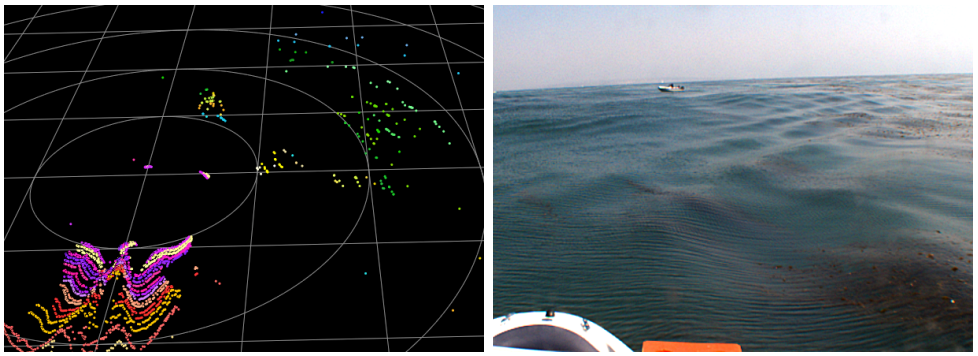

(a) LIDAR return (b) Photo

Figure 7: Return from kelp at the sea surface between approximately 10 and 30 meters

aerated water and other benign returns while remaining sensitive to smaller obstacles which may still pose a threat.

A simple obstacle detection scheme can be implemented by monitoring the statistics of laser returns binned on grid. We use a 3 meter square grid in this example. This sample scene includes the moving test platform, two additional boats at about 30 and 40 meters, wakes for all three boats, and radar induced noise (see section 4.1). For reference, the raw HDL-64E scene is displayed in Figure 9. Figures 8a-8d show such grids for the mean and variance of return height and intensity. Figure 8e indicates the number of laser returns falling into each bin (darker is higher number). An obstacle map is constructed in Figure 8f by thresholding on the height variance and applying a mask dependent on range and the number of returns; a polar grid could be used to remove the range dependence. This simple method discriminates between returns from wakes and the boats themselves and filters the sparse returns induced by electromagnetic interference from the RADAR.

## 4. COMPLICATIONS

While the sensor has operated very well in the harsh marine environment, a number of complications have arisen. This section discusses a few of them including electromagnetic and network interference, calibration, and laser reliability.

### 4.1 Electromagnetic and network interference

Two-way electromagnetic interference has been observed wherein the HDL-64E affects GPS receivers and is affected by marine RADAR pulses. GPS interference is mitigated by raising the antenna above the height of the LIDAR.

(a) Height mean (darker is lower)

(b) Height variance

(c) Intensity mean

(d) Intensity variance

(e) Number of returns

(f) Obstacle map from height variance and a range-dependent mask on the number of returns

Figure 8: Automated obstacle map generation

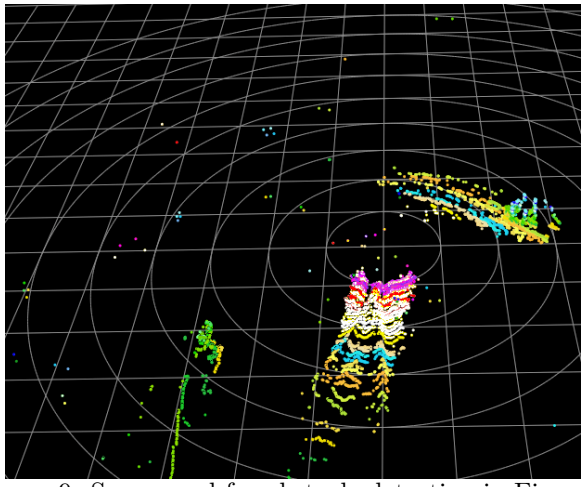

Figure 9: Scene used for obstacle detection in Figure 8

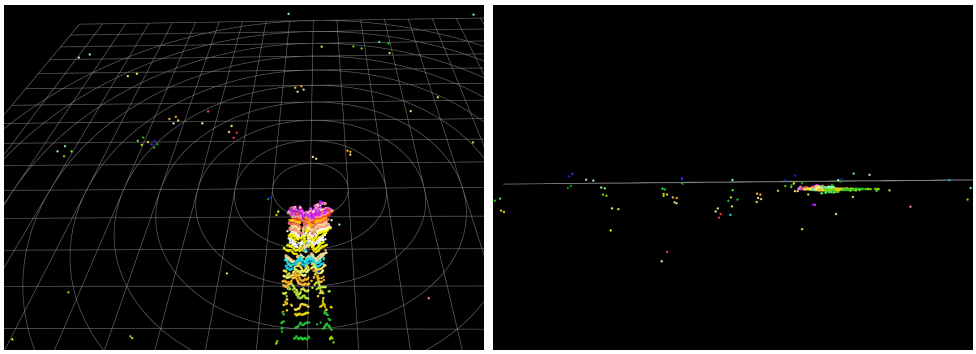

(a) Horizontal spread (b) Vertical spread

Figure 10: LIDAR plot showing horizontal (10a) and vertical (10b) spread of typical RADAR-induced noisy returns.

Our test platform has a standard marine RADAR antenna in proximity to the LIDAR. We have noticed that the RADAR induces noise in the LIDAR data. The horizontal and vertical spreads of RADAR-induced noise are illustrated in Figures 10a and 10b respectively. This data is taken from clear, calm sea surface so returns besides those of the wake are deemed noise. The occurrence of this noise is periodic with the spin rate of the RADAR antenna. Because of its periodic occurrence and its random height profile, this noise is relatively simple to filter.

Another type of interference arises because the sensor data is sent via an Ethernet interface and packaged in UDP broadcast packets. This makes receiving the data simple, but makes network isolation—either physical or through router configuration—necessary. Absent isolation, the high packet rate causes UDP broadcast flooding.

### 4.2 Calibration and reliability

Multi-laser scanners are difficult to accurately calibrate. Each of the 64 lasers in the HDL-64E is calibrated according to five parameters. Errors in any of these parameters lead to mispositioned data points and, subsequently, difficulties for algorithms that rely on accuracy and consistency between lasers such as plane fitting and landmark extraction. While the HDL-64E is calibrated by the manufacturer, the supplied calibration parameters do not always provide sufficient results.

To illustrate mis-calibration effects in our particular unit, Figure 11 shows views of the mural-painted San Diego National Bank wall using the manufacturer-supplied calibration parameters. Because some of the calibration errors are range dependent, imaging this large planar surface at a significant distance (40 meters) allows the mis-calibration to be easily seen. Figure 11a shows depth spreading in the surface of the wall as viewed from the top. Ideally, all laser returns from the wall would align. Figure 11b shows a glancing view of this same collection from the right side. Here, the relative offsets between lasers is readily apparent. For reference, Figures 11c and 11d show the LIDAR return viewed from the front and a photo of the wall.

The complications of and an optimization-based technique for multi-beam LIDAR calibration are considered by Muhammad and Lacroix.[4] The Ben Franklin Racing Team from the Urban Challenge also noticed mis-calibrations in their sensor and attempted to account for them through additional distance offset parameters obtained through comparison with SICK LMS-291 LIDAR readings.[5]

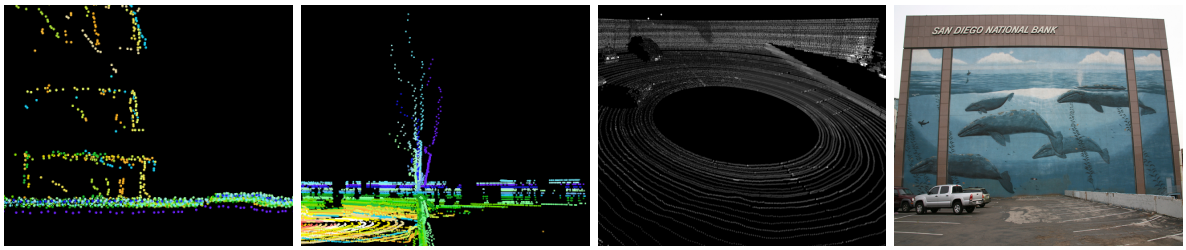


(a) Top view (right end of wall) (b) Side view (from the right side) (c) Front face (d) Photo

Figure 11: Mis-calibration illustrated by glancing views of a 40 m distant flat wall seen from the top and the side

## REFERENCES


1. Velodyne Lidar Inc., *HDL-64E User's Manual*. Velodyne Lidar Inc. 345 Digital Drive, Morgan Hill, CA 95037, 2008.
2. C. Urmson *et al.*, "Autonomous driving in urban environments: Boss and the Urban Challenge," *Journal of Field Robotics Special Issue on the 2007 DARPA Urban Challenge* **Vol. 25, Issue. 8**, pp. 425–466, 2008.
3. M. Montemerlo *et al.*, "Junior: The Stanford entry in the Urban Challenge," *Journal of Field Robotics Special Issue on the 2007 DARPA Urban Challenge* **Vol. 25, Issue. 9**, pp. 569–597, 2008.
4. N. Muhammad and S. Lacroix, "Calibration of a rotating multi-beam lidar," tech. rep., Laboratory for Analysis and Architecture of Systems, 2009.
5. J. Bohren *et al.*, "Little Ben: The Ben Franklin Racing Team's entry in the 2007 DARPA Urban Challenge," *Journal of Field Robotics Special Issue on the 2007 DARPA Urban Challenge* **Vol. 25, Issue 9**, pp. 598–614, 2008.